Covalently Linked Donor–Acceptor Cyclometalated Platinum(II) Complexes. Structure and Luminescent Properties

Chin-Wing Chan, Ting-Fong Lai, Chi-Ming Che,* and Shie-Ming Peng‡

Contribution from the Departments of Chemistry, The University of Hong Kong, Pokfulam Road, Hong Kong

*Received February 8, 1993**

Abstract: Reaction of $[Pt(CH_3CN)_4]^{2+}$ with 2,9-diphenyl-1,10-phenanthroline (dpp) in acetonitrile gave the cyclometalated complex $[Pt(C^N^N\text{-dpp})(CH_3CN)](ClO_4)$ {here abbreviated as **[7]**(ClO_4)}, the structure of which has been established by ^1H–^1H COSY and X-ray crystallography: triclinic, $P\bar{1}$, a = 13.322(3) Å, b = 13.877(3) Å, c = 14.164(6) Å, α = 86.74(3)°, β = 105.87(3)°, γ = 108.93(2)°, V = 2381.0(12) Å^3, Z = 2. The resemblance between solution excimeric emission and solid-state emission of **7** suggests that the structure of excimer $[\mathbf{7}]_2$* in CH_2Cl_2 is similar to the dimeric unit in the crystalline state. The coordinated CH_3CN in **7** is substitution labile and can be easily replaced by nitrogen bases upon heating in acetone to give covalently-linked donor–acceptor organometallic complexes. Crystal structures of coordinated 4-(4-nitrobenzyl)pyridine and 4-(2-(9-anthryl)vinyl)pyridine substituted complexes (**10** and **11**, respectively) have been determined: **[10]**(ClO_4), triclinic, $P\bar{1}$, a = 10.143(2) Å, b = 13.025(4) Å, c = 13.581(2) Å, α = 68.64(2)°, β = 77.15(2)°, γ = 68.00(2)°, V = 1541.6(7) Å^3, Z = 2; **[11]**(ClO_4), monoclinic, $P2_1/c$, a = 13.065(4) Å, b = 18.647(5) Å, c = 16.276(4) Å, β = 116.59(2)°, V = 3546(3) Å^3, Z = 4. In both structures, one of the phenyl rings of $(C^N^N\text{-dpp})$ is nearly parallel with the nitrogen base ligand, which is perpendicular to the mean plane defined by the atoms N(1), N(2), C(13), and Pt. The photoluminescent properties of **7** and complexes with covalently linked organic quenchers are described.

Introduction

There is an upsurge of interest in new supramolecular transition-metal complexes built from luminescent inorganic complexes and organic quenchers.[1,2] A number of such covalently linked luminophore–quencher complexes, where the luminophore is a d^6 metal polypyridine fragment, are known.[2] However, those complexes with organometallic luminophores are sparse.[3] Recently, Gray and co-workers[4] reported a series of synthetic pyrazolate-bridged Ir(I) dimers covalently linked to pyridinium acceptors. These donor–acceptor iridium complexes have been found to undergo photo-induced electron-transfer reactions with rate constants falling in the Marcus inverted region at high driving force.[4] Herein is described a convenient entry into a new class of donor–acceptor complexes consisting of cyclometalated Pt(II) luminophores[5] and organic quenchers. It has long been recognized that cyclometalated complexes possess interesting photophysical and photochemical properties.[6] Donor–acceptor platinum(II) complexes are of special interest in molecular recognition reactions because of the coordinative unsaturated nature of the Pt(II) center.

Experimental Section

Materials. The ligand 2,9-diphenyl-1,10-phenanthroline (dpp) was prepared as a pale yellow solid by the reported procedure.[7] Acetonitrile was purified according to literature methods.[8] $PtCl_2$ was purchased from Strem Chemicals. Acetone for photophysical measurements was of GR grade (E. Merck) and did not show any luminescence under measuring conditions. Dichloromethane was freshly distilled from P_2O_5. All other reagents were used as received.

Physical Measurements. Infrared spectra were obtained in KBr pellets on a Nicolet 20 SXC FT-IR spectrometer. UV–visible spectra were obtained on a Milton Roy Spectronic 2000 spectrophotometer. Proton NMR spectra were obtained on a JEOL GSX 270 FT-NMR spectrometer with TMS as an internal standard. Elemental analyses were performed at the Shanghai Institute of Organic Chemistry, Chinese Academy of Science.

Cyclic voltammograms were measured using a PAR Model 273 potentiostat coupled to a Kipp & Zonen X-Y recorder. A conventional two compartment cell was used in nonaqueous measurements with silver–silver nitrate (0.1 M in acetonitrile) as the reference electrode. The working electrode was made of glassy carbon. The electrode surface was treated as described before.[9]

‡ National Taiwan University, Taipei, Taiwan.

* Abstract published in *Advance ACS Abstracts*, October 1, 1993.

(1) (a) Balzani, V.; Scandola, F. *Supramolecular Photochemistry*; Ellis Horwood Ltd.: New York, 1991. (b) Collin, J. P.; Guillerez, S.; Sauvage, J.-P.; Barigelletti, F.; De Cola, L.; Flamigui, L.; Balzani, V. *Inorg. Chem.* **1991**, *30*, 4230–4238.

(2) For examples, see: (a) Mocklenburg, S. L.; Peak, B. M.; Erickson, B. W.; Meyer, T. J. *J. Am. Chem. Soc.* **1991**, *113*, 8540–8542. (b) Chen, P.; Duesing, R.; Graff, D. K.; Meyer, T. J. *J. Phys. Chem.* **1991**, *95*, 5850–5858. (c) Furue, M.; Naiki, M.; Kanamatsu, Y.; Kushida, T.; Kamachi, M. *Coord. Chem. Rev.* **1991**, *111*, 221–226.

(3) (a) MacQueen, D. B.; Eyler, J. R.; Schanze, K. S. *J. Am. Chem. Soc.* **1992**, *114*, 1897–1898. (b) Perkins, T. A.; Hauser, B. T.; Eyler, J. R.; Schanze, K. S. *J. Phys. Chem.* **1990**, *94*, 8745–8748.

(4) Fox, L. S.; Koik, M.; Winkler, J. R.; Gray, H. B. *Science* **1990**, *247*, 1069–1071.

(5) (a) Maestri, M.; Deuschel-Cornioley, C.; von Zelewsky, A. *Coord. Chem. Rev.* **1991**, *111*, 117–123. (b) Deuschel-Cornioley, C.; Lüond, R.; von Zelewsky, A. *Helv. Chim. Acta* **1989**, *72*, 377–382. (c) Chassot, L.; Müller, E.; von Zelewsky, A. *Inorg. Chem.* **1984**, *23*, 4249–4253.

(6) (a) King, K. A.; Spellane, P. J.; Watts, R. J. *J. Am. Chem. Soc.* **1985**, *107*, 1431–1432. (b) Barigelletti, F.; Sandrini, D.; Maestri, M.; Balzani, V.; von Zelewsky, A.; Chassot, L.; Jolliet, P.; Maeder, U. *Inorg. Chem.* **1988**, *27*, 3644–3647. (c) Schwarz, R.; Gliemann, G.; Chassot, L.; Jolliet, P.; von Zelewsky, A. *Helv. Chim. Acta* **1989**, *72*, 224–236. (d) Collin, J.-P.; Beley, M.; Sauvage, J.-P.; Barigelletti, F. *Inorg. Chim. Acta* **1991**, *186*, 91–93. (e) Blanton, C. B.; Murtaza, Z.; Shaver, R. J.; Rillema, D. P. *Inorg. Chem.* **1992**, *31*, 3230–3235.

(7) Dietrich-Buchecker, C. D.; Marnot, P. A.; Sauvage, J. P. *Tetrahedron Lett.* **1982**, *23*, 5291–5294.

(8) Perrin, D. D.; Armarego, W. L. F.; Perrin, D. R. *Purification of Laboratory Chemicals*, 2nd ed.; Pergamon Press: New York, 1980; pp 79–81.

(9) Che, C.-M.; Wong, K.-Y.; Anson, F. C. *J. Electroanal. Chem. Interfacial Electrochem.* **1987**, *226*, 211–226.

0002-7863/93/1515-11245$04.00/0

Chart I

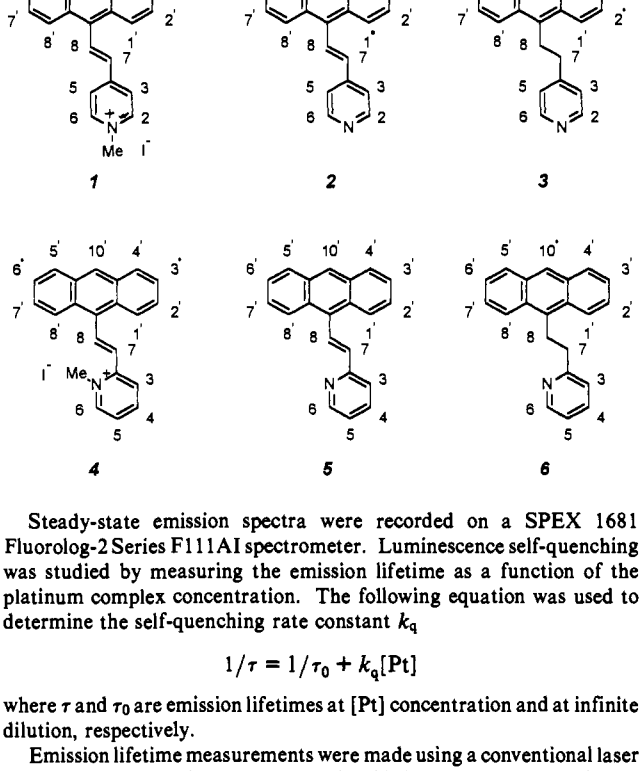

Steady-state emission spectra were recorded on a SPEX 1681 Fluorolog-2 Series F111AI spectrometer. Luminescence self-quenching was studied by measuring the emission lifetime as a function of the platinum complex concentration. The following equation was used to determine the self-quenching rate constant k_q

$$1/\tau = 1/\tau_0 + k_q[\mathrm{Pt}]$$

where τ and τ_0 are emission lifetimes at [Pt] concentration and at infinite dilution, respectively.

Emission lifetime measurements were made using a conventional laser system. The excitation source was the third harmonic (355 nm) of a Quanta-Ray Q-switched DCR-3 pulsed Nd-YAG laser (10 Hz, G-resonator). Laser power was kept below 10% to avoid excited-state annihilations. The signals were recorded on a Tektronix Model 2430 digital oscilloscope and analyzed using a least-squares fit program. The quantum yield of emission was measured by the method of Crosby[10] with $[Ru(bpy)_3](PF_6)_2$ in degassed acetonitrile as the standard ($\phi_f = 0.062$ at room temperature[11]) and calculated using the following equation

$$\left(\frac{\phi_s}{\phi_r}\right) = \left(\frac{B_r}{B_s}\right)\left(\frac{n_s^2}{n_r^2}\right)\left(\frac{D_s}{D_r}\right)$$

where ϕ = emission quantum yield, n = refractive index, D = integration, $B = 1 - 10^{-AL}$ (A = absorption and L = light path in solution), and s and r stand for sample and reference, respectively. Solutions for photophysical measurements were degassed with no fewer than three freeze–pump–thaw cycles.

1-Methyl-4-(2-(9-anthryl)vinyl)pyridinium Iodide (1)[12] (Chart I). A mixture of 9-anthraldehyde (1 g, 4.85 mmol), 1,4-dimethylpyridinium iodide (1.14 g, 1 equiv), and piperidine (0.4 g, 1 equiv) in absolute ethanol (20 mL) was heated at 60 °C for 1 h and cooled. Bright orange microcrystals were filtered out and washed with a few milliliters of cooled absolute ethanol. The yield was about 90%. ^{1}H NMR ($CDCl_3$): δ 9.13–9.10 (d, H2, 6), 8.70–8.64 (m, H1′,8′), 8.53 (s, H10′), 8.18–8.14 (d, H3,5), 8.70–8.64 (d, H7, $^3J_{trans}$ = 17 Hz), 7.18–7.12 (d, H8, $^3J_{trans}$ = 17 Hz), 8.08–8.04 (m, H4′,5′), 7.60–7.50 (m, H2′,3′,6′,7′), 4.65 (s, N–Me). IR (cm^{-1}): 1638 s, 1610 s, 1185 m, 990 m, 890 m, 840 m, 820 m, 730 s, 500 s.

4-(2-(9-Anthryl)vinyl)pyridine (2).[13] A mixture of 1-methyl-4-(2-(9-anthryl)vinyl)pyridinium iodide (1.9 g, 4.49 mmol) and triphenylphosphine (4.7 g, 4 equiv) in dimethylformamide (20 mL) was refluxed for 12 h. The resulting mixture was evaporated to dryness under vacuum. The desired product was isolated in 60% yield after column chromatography (petroleum ether (bp 60–80 °C)/ethyl acetate (1:1), R_f = 0.25) on silica gel (product can be recrystallized in a hexane/acetone mixture). Anal. Calcd for $C_{21}H_{15}N$: C, 89.56; H, 5.33; N, 4.98. Found: C, 89.31; H, 5.26; N, 4.92. ^{1}H NMR ($CDCl_3$): δ 8.69–8.67 (m, H2,6), 8.44 (s, H10′), 8.24–8.30 (m, H1′,8′), 8.17–8.11 (d, H7, $^3J_{trans}$ = 16.4 Hz), 8.06–8.00 (m, H4′,5′), 7.53–7.51 (m, H3,5), 7.46–7.51 (m, H2′,3′,6′,7′), 6.93–6.87 (d, H8). IR (cm^{-1}): 1590 s, 1410 m, 990 m, 980 m, 890 s, 830 m, 780 m, 730 s.

4-(2-(9-Anthryl)ethyl)pyridine (3). A mixture of 4-(2-(9-anthryl)-vinyl)pyridine (176 mg, 0.63 mmol) and Pd/C (5%, 20 mg) in anhydrous methanol (15 mL) was stirred under a pressure of 1 atm of hydrogen at room temperature. After 3 h, the reaction mixture was filtered through Celite and evaporated under reduced pressure. The desired product was isolated in 70% yield after recrystallization in acetone. Anal. Calcd for $C_{21}H_{17}N$: C, 89.65; H, 5.37; N, 4.98. Found: C, 87.67; H, 5.72; N, 4.77. ^{1}H NMR ($CDCl_3$): δ 8.54–8.51 (m, H2,6), 8.37 (s, H10′), 8.21–8.18 (H1′,8′), 8.03–8.00 (dd, H4′,5′), 7.54–7.43 (m, H2′,3′,6′,7′), 7.23–7.21 (m, H3,5), 3.92–3.86 (H8), 3.10–3.03 (m, H7). IR (cm^{-1}): 1621 m, 1601 s, 1559 m, 1446 m, 1412 m, 890 m, 846 m, 805 m, 785 m, 736 s, 496 s.

1-Methyl-2-(2-(9-anthryl)vinyl)pyridinium Iodide (4). A mixture of 1,2-dimethylpyridinium iodide (1 g, 4.26 mmol), 9-anthraldehyde (1 equiv), and piperidine (1 equiv) in absolute ethanol (20 mL) was heated to 80 °C for 10 min. Then the solution was reduced to ~10 mL and cooled. Bright orange microcrystals were filtered out and washed with a few milliliters of cooled absolute ethanol. The yield was 64%.

2-(2-(9-Anthryl)vinyl)pyridine (5). A mixture of 1-methyl-2-(2-(9-anthryl)vinyl)pyridinium iodide (1.15 g, 2.72 mmol) and triphenylphosphine (2.8 g, 4 equiv) in DMF (30 mL) was refluxed at 160 °C for 16 h. The cooled mixture was poured into an equal volume of water and extracted with diethyl ether (3 × 30 mL). The organic layer was dried over anhydrous sodium sulfate and evaporated to dryness. Column chromatography of the residue on silica gel (70–230 mesh) with petroleum ether (bp 60–80 °C)/ethyl acetate (4:1; R_f = 0.5) afforded the desired product in 59% yield. Anal. Calcd for $C_{21}H_{15}N$: C, 89.56; H, 5.33; N, 4.98. Found: C, 88.60; H, 5.31; N, 4.80. ^{1}H NMR ($CDCl_3$): δ 8.72–8.71 (m, H6), 8.66–8.60 (dd, H7, $^3J_{trans}$ = 16.4 Hz), 8.56 (s, H10′), 8.42–8.10 (m, A_2B_2, H1′,4′,5′,8′), 7.90–7.83 (dt, H5), 7.69–7.65 (d, H3), 7.58–7.51 (m, A_2B_2, H2′,3′,6′,7′), 7.37–7.32 (ddd, H4), 7.13–7.07 (d, H8, $^3J_{trans}$ = 16.4 Hz). IR (cm^{-1}): 1581 m, 1562 m, 1472 m, 1433 m, 980 m, 972 m, 884 m, 840 m, 789 m, 763 s, 734 s.

2-(2-(9-Anthryl)ethyl)pyridine (6). A mixture of 2-(2-(9-anthryl)-vinyl)pyridine (105 mg, 0.37 mmol) and Pd/C (5%, 20 mg) was stirred in anhydrous methanol (15 mL) under a pressure of 1 atm of hydrogen for 12 h. Filtration and evaporation under reduced pressure afforded the title compound in 70% yield. Anal. Calcd for $C_{21}H_{17}N$: C, 89.65; H, 5.37; N, 4.98. Found: C, 83.43; H, 5.41; N, 4.59. ^{1}H NMR ($CDCl_3$): δ 8.67–8.64 (m, H6), 7.60–7.54 (dt, H5), 7.16–7.11 (ddd, H4), 7.07–7.04 (d, H3), 4.07–4.01 (m, H7), 3.29–3.23 (m, H8), 8.34–8.30, 8.02–7.98 (A_2B_2, H1′,4′,5′,8′), 7.52–7.40 (A_2B_2, H2′,3′,6′,7′), 8.35 (s, H10′). IR (cm^{-1}): 1589 m, 1566 m, 1489 m, 1432 m, 885 m, 771 m, 755 m, 727 s, 492 m. UV–vis (acetone) λ_{max} (10^{-3} ϵ): (350, 6.26), (368, 9.71), (388, 9.43).

[Pt(C^N^N-dpp)(CH$_3$CN)](ClO$_4$) {[7](ClO$_4$)}. A mixture of bis(acetonitrile)dichloroplatinum(II) (0.23 g, 0.66 mmol) and silver perchlorate (dry in P_2O_5; 0.27 g, 2 equiv) in acetonitrile (25 mL) was refluxed until the solution became colorless (about 3 h). Then the solution was filtered through Celite to remove the insoluble AgCl. The tetrakis(acetonitrile)-platinum(II) perchlorate prepared above was added to a refluxing acetonitrile solution (15 mL) of dpp (0.44 g, 2 equiv), and the resulting solution was refluxed for 1 day. An orange precipitate was filtered out. Diffusion of diethyl ether into the acetonitrile solution of **7** afforded deep-red needles (yield 12%). Anal. Calcd for $PtC_{26}H_{18}N_3ClO_4$: C, 46.82; H, 2.72; N, 6.30. Found: C, 46.63; H, 2.56; N, 6.64. ^{1}H NMR (DMF-d_6): δ 8.92–8.20 (dd, H8,13), 8.70–8.20 (dd, H9,12), 8.20–8.10 (dd, H10,11), 7.90 (m, H16,20), 7.75 (m, H17,18,19), 7.68 (dd, H5), 7.12 (m, H3,4), 6.96 (m, H2), 2.23 (t, H–CH$_3$CN, $^4J_{Pt-H}$ = 20.5 Hz). IR (cm^{-1}): 1624 m, 1584 m, 1147 s, 1117 s, 1086 s, 862 m, 765 m, 736 m, 704 m, 637 m, 624 s. UV–vis (CH$_3$CN) λ_{max} (10^{-3} ϵ): (205, 39.7), (251, 35.2), (268, 29.6), (333, 24.1), (374, 4.8), (439, 0.87).

[Pt(C^N^N-dpp)(L)](ClO$_4$) (8–13) (Chart II). A mixture of excess (ortho/para) substituted pyridine (L) and [7](ClO$_4$) (50 mg, 7.5 × 10^{-2} mmol) was heated in boiling acetone (50 mL) for 30 min. The mixture was hot-filtered, and the filtrate was evaporated to 25 mL. Diethyl ether (about three times the volume of acetone) was layered onto the cool filtrate, which was then kept at 4 °C. The precipitate was isolated as light orange to yellow powder on sintered glass, washed with a few milliliters of diethyl ether, and dried under vacuum. The yield was about 60–70%. Analyses for **8**, **9**, **11–13** are listed in Table I. All samples have been checked by ^{1}H NMR for the presence of free substituted pyridine.

(10) Demas, J. N.; Crosby, G. A. *J. Phys. Chem.* **1971**, *75*, 991–1024.
(11) Calvert, J. M.; Caspar, J. V.; Binstead, R. A.; Westmoreland, T. D.; Meyer, T. J. *J. Am. Chem. Soc.* **1982**, *104*, 6620–6627.
(12) Jerchel, D.; Heck, H. E. *Justus Liebigs Ann. Chem.* **1958**, *613*, 171.
(13) Hart, L. S. *J. Chem. Soc., Chem. Commun.* **1979**, 24–25.

Chart II

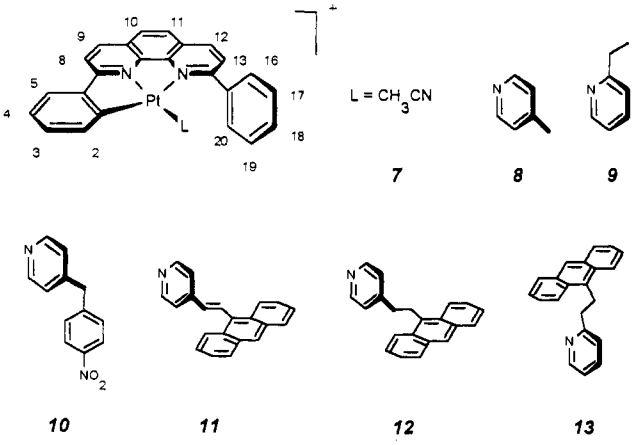

X-ray Structure Determination. Crystals of [**7**](ClO_4) suitable for diffraction analysis were obtained from acetonitrile solution. A crystal was mounted in a sealed capillary. Diffraction measurements were carried out on a Nonius CAD-4 fully automated four-circle diffractometer at National Taiwan University. The unit cell was determined and refined using setting angles of 25 reflections, with 2θ angles in the range of 2–44.9°. All data reduction and structure refinement were performed using the NMRR-SDP-VAX packages. The structure was solved by the Patterson method and refined by least-squares; all non-hydrogen atoms were refined with anisotropic thermal parameters. The final difference map contained a maximum at 0.64 e/Å^3 and a minimum at –0.64 e/Å^3. Selected bond lengths and bond angles are listed in Table III.

X-ray diffraction data of [**10**](ClO_4) and [**11**](ClO_4) were collected on an Enraf-Nonius diffractometer with graphite monochromated Mo Kα radiation at The University of Hong Kong. The unit-cell dimensions were obtained from a least-squares fit of 25 reflections in the range of $23° < 2\theta < 31°$ for **10** and $23° < 2\theta < 34°$ for **11**. The data were corrected for Lorentz, polarization, and absorption effects. The empirical absorption correction was based on azimuthal (ψ) scans of nine reflections with $80° < \chi < 90°$. Atomic scattering factors were taken from the International Tables for X-ray Crystallography, Vol. IV (1974), and all calculations were carried out on a Micro Vax II computer using the Enraf-Nonius structure determination package, SDP (1985).[14] The structures were solved by Patterson and Fourier methods and refined by full-matrix least-squares. All the non-hydrogen atoms were refined anisotropically, and the hydrogen atoms at calculated positions with assigned isotropic temperature factors were not refined. The final R factors were given in Table II. The final difference map for **10** was featureless, but for **11**, residual densities of 3.8, 2.4, 1.8, –1.9, and –1.4 eÅ^{-3} were observed at distances approximately 1 Å from the Pt atom, and this might be the result of imperfect absorption correction. Selected bond lengths and bond angles are listed in Table IV. The data collection parameters and crystal structural data are summarized in Table II.

Results and Discussion

Synthesis of the Cyclometalated Platinum Complex. The preparation of metal complexes with labile coordinated solvent molecules as precursors for further syntheses poses a challenge to coordination chemists. An attempted synthesis of **7** in a refluxing water/acetonitrile mixture of dpp and K_2PtCl_4 was unsuccessful. Protonated dpp was recovered in most cases. Cyclometalation of 2,9-diphenyl-1,10-phenanthroline (dpp) was brought about as an inadvertent bonus when platinum(II) perchlorate and dpp were heated in acetonitrile. The bright orange precipitate recovered after purification showed intense room-temperature luminescence upon UV irradiation.

The reaction is believed to proceed by an electrophilic pathway where a platinum(II)–π(arene) complex may be involved,[15] which collapses into a platinum cyclohexadienyl cation. Proton abstraction from the cyclohexadienyl cation is facilitated with excess dpp. Addition of 2 equiv of free base therefore shortens the reaction time to 1 day.

The coordinated CH_3CN in **7** is substitutionally labile and is easily replaced by a nitrogen base upon heating in acetone for 1–2 h. Complexes **8**–**13** have been prepared in this manner (Chart II). Construction of donor–acceptor molecules based on pyridine coordinated metalloporphyrin systems has been reported previously.[16]

^{1}H–^{1}H COSY of 7 in Dimethylformamide (DMF). The assignment of the resonance position for the ring protons on **7** is facilitated with correlation NMR spectroscopy. As shown in Figure 1, δ 6.5–9.0 covers all the aromatic proton resonance signals. The off-diagonal signals can be separated into three groups: (a) δ 6.9–7.7, (b) δ 7.75–7.95, and (c) δ 8.05–8.95. The most downfield signals can be assigned to protons on phenanthroline in which one AB and two AX systems can be recognized. The splitting arises from the nonequivalency of phenyl rings upon metalation. The decrease in the number of differences in the chemical environment experienced by protons H8 and H13, H9 and H12, and H10 and H11 leads to the increase of $J/\Delta\delta$ values. While the coupling constants of these three sets of protons are almost the same, $\Delta\delta$'s for H8 and H13, H9 and H12, and H10 and H11 decrease progressively.

Groups a and b exhibit hyperfine splitting and should correspond to protons on the phenyl ring. By integration, group a is subdivided into 1H and 2H and 1H, while group b is separated into 3H and 2H. On the basis of symmetry arguments, group b should originate from the protons on the pending phenyl ring, namely, H16 and H20 and H17, H18, and H19. Protons H3 and H4 in group a are characterized by triplet splitting with two neighboring protons. The observed multiples are due to the similarities in their chemical shifts. The two single protons in group a are distinguished by the large three-bond coupling constant of H2 with ^{195}Pt ($^3J_{Pt}$ = 27 Hz, not shown). The more upfield signal is therefore assigned H2.

After coordination with pyridine-type ligands or other heteroaromatics, H2 is in the shielding region and experiences an upfield shift ($\delta \leq 6$ ppm). Together with the hyperfine coupling with the ^{195}Pt isotope, the resonance signal of H2 serves as a benchmark for a stable donor–acceptor pair in the solution state (photophysical studies in solution have used ^{1}H NMR to confirm stable adducts in a variety of solvents).

Structures of [Pt(C^N^N-dpp)(NCCH$_3$)](ClO$_4$) {[7](ClO$_4$)} and 4-(4-Nitrobenzyl)- and 4-(2-(9-Anthryl)vinyl)pyridine Adducts {[10](ClO$_4$) and [11](ClO$_4$), respectively}. It has been demonstrated that cyclometalated platinum(II) complexes crystallize in stacking columnar structures.[5c,17a] Extra phenyl ring substitution in **7** results in an unusual discrete platinum dimer (Figure 2). The platinum(A)–platinum(B) distance was found to be 3.37 Å with two phenanthroline moieties being held in an almost face-to-face orientation and with the Pt(A)–Pt(B) vector perpendicular to both aromatic planes. It is interesting to note that the two phenyl rings in free dpp are coplanar with phenanthroline and stacked on each other at a separation of 3.373(9) Å.[18] While phenanthroline stacking in free dpp offsets dipole–dipole repulsion by avoiding nitrogen atoms directly overlaying on each other, the Pt(A)–Pt(B) vector in **7** has the same closest dpp separation with N(1A) and N(1B) in an almost eclipsed position. These structural features suggest the presence of weak metal–metal interactions and ligand π–π interactions in the dimer.

(14) *International Tables for X-Ray Crystallography*; Kynoch Press: Birmingham, U.K., 1974; Vol. 4, pp 99–149. *Enraf-Nonius Structure Determination Package, SDP*; Enraf-Nonius: Delft, The Netherlands, 1985.
(15) Constable, E. C. *Polyhedron* **1984**, *3*, 1037–1057.
(16) Hunter, C. A.; Sanders, J. K. M.; Beddard, G. S.; Evans, S. *J. Chem. Soc., Chem. Commun.* **1989**, 1765–1767.
(17) (a) Constable, E. C.; Henney, R. P. G.; Leese, T. A.; Tocher, D. A. *J. Chem. Soc., Chem. Commun.* **1990**, 513–515. (b) Constable, E. C.; Henney, R. P. G.; Raithby, P. R.; Sousa, L. R. *J. Chem. Soc., Dalton Trans.* **1992**, 2251–2258.
(18) Klemens, F. K.; Palmer, C. E. A.; Rolland, S. M.; Fanwick, P. E.; McMillin, D. R.; Sauvage, J.-P. *New J. Chem.* **1990**, *14*, 129–133.

Table I. Elemental Analyses for Pyridine Adducts **8**, **9**, and **11–13**

no.	formula (fw)	% calcd C	% calcd H	% calcd N	% found C	% found H	% found N
8	$C_{30}H_{22}N_3PtClO_4$ (719.06)	50.11	3.08	5.84	50.14	3.19	5.24
9	$C_{31}H_{24}N_3PtClO_4$ (733.11)	50.79	3.31	5.73	50.48	3.04	5.60
11	$C_{45}H_{30}N_3PtClO_4$ (906.16)	59.56	3.31	4.63	58.44	3.00	4.44
12	$C_{45}H_{32}N_3PtClO_4$ (908.16)	59.46	3.52	4.62	58.28	3.17	4.37
13	$C_{45}H_{32}N_3PtClO_4$ (908.16)	59.46	3.52	4.62	59.79	3.52	4.31

Table II. Summary of Crystal Data, Intensity Collection, and Structure Refinement Parameters for [**7**](ClO_4), [**10**](ClO_4), and [**11**](ClO_4)

	[**7**](ClO_4)	[**10**](ClO_4)	[**11**](ClO_4)
formula	$Pt_2C_{54}H_{39}N_7Cl_2O_8$	$PtC_{36}H_{25}N_4ClO_6$	$PtC_{45}H_{30}N_3ClO_4$
fw	1375.02	840.16	907.30
crystal system	triclinic	triclinic	monoclinic
space group	$P\bar{1}$	$P\bar{1}$	$P2_1/c$
a, Å	13.322(3)	10.143(2)	13.065(4)
b, Å	13.877(3)	13.025(4)	18.647(5)
c, Å	14.164(6)	13.581(2)	16.276(4)
α, deg	86.74(3)	68.64(2)	90
β, deg	105.87(3)	77.15(2)	116.59(2)
γ, deg	108.93(2)	68.00(2)	90
V, Å^3	2381.1(1)	1541.6(7)	3546(3)
Z	2	2	4
ρ_{calcd}, g/cm^3	1.918	1.810	1.7
μ(Mo Kα), cm^{-1}	61.1	47.38	41.2
$F(000)$	1332	824	1792
$R(\|F_o\|)^a$	0.035	0.022	0.055
$R_w(\|F_o\|)^a$	0.033	0.029	0.063
S^a	1.23	1.04	1.62

^{a} $R = \sum\|F_o\| - |F_c\|/\sum|F_o|$. $R_w = [w(|F_o| - |F_c|)^2/\sum w|F_o|^2]^{1/2}$, with $w = 4F_o^2/[\sigma^2(F_o^2) + (0.04F_o^2)^2]$. $S = [\sum w(|F_o| - |F_c|)^2/(m-p)]^{1/2}$.

Table III. Selected Bond Lengths (Å) and Bond Angles (deg) for [**7**](ClO_4)

Bond Lengths			
Pt(A)–Pt(B)	3.3724(9)		
Pt(A)–N(1A)	2.231(8)	Pt(B)–N(1B)	2.193(8)
Pt(A)–N(2A)	1.940(8)	Pt(B)–N(2B)	1.913(8)
Pt(A)–N(3A)	1.970(9)	Pt(B)–N(3B)	1.981(8)
Pt(A)–C(13A)	2.00(1)	Pt(B)–C(13B)	1.97(1)
Bond Angles			
Pt(B)–Pt(A)–N(1A)	87.2(2)	Pt(A)–Pt(B)–N(1B)	89.3(2)
Pt(B)–Pt(A)–N(2A)	85.9(2)	Pt(A)–Pt(B)–N(2B)	95.6(2)
Pt(B)–Pt(A)–N(3A)	96.8(3)	Pt(A)–Pt(B)–N(3B)	80.7(2)
Pt(B)–Pt(A)–C(13A)	93.7(3)	Pt(A)–Pt(B)–C(13B)	95.8(3)
N(1A)–Pt(A)–N(2A)	78.6(3)	N(1B)–Pt(B)–N(2B)	79.3(3)
N(2A)–Pt(A)–N(3A)	173.2(3)	N(2B)–Pt(B)–N(3B)	175.1(3)
N(2A)–Pt(A)–C(13A)	81.4(4)	N(2B)–Pt(B)–C(13B)	81.6(4)
N(1A)–Pt(A)–N(3A)	107.8(3)	N(1B)–Pt(B)–N(3B)	103.7(3)
N(1A)–Pt(A)–C(13A)	159.8(4)	N(1B)–Pt(B)–C(13B)	160.6(4)
N(3A)–Pt(A)–C(13A)	92.2(4)	N(3B)–Pt(B)–C(13B)	95.6(4)

Analogous dimeric structures have also been observed,[5c,17a] but the Pt–Pt vectors in those cases are inclined with respect to two parallel planes of the aromatic ligands. In complex **7**, the two Pt–C⌒N⌒N planes are slightly twisted around the Pt(A)–Pt(B) axis, since the presence of a pending phenyl substituent limits the dihedral angle between the two coordinated acetonitrile molecules.

The Pt–C bond distances [2.00(1) Å] are in agreement with those reported previously.[5c,17a] However, the rigidity of phenanthroline prevents ring distortion so that the platinum–nitrogen distances in **7** are slightly longer than those corresponding distances in [Pt(L)(CH_3CN)](PF_6) (HL = 6-phenyl-2,2′-bipyridine).[17a]

The out-of-plane conformation of the pending phenyl ring with regard to the Pt–C(13)–N(1)–N(2) plane is due to repulsive interaction with coordinated acetonitrile. A similar conformation of dpp has been reported for the structure of $Cu(dpp)_2^+$,[18] in which the average torsion angle between phenanthroline and the phenyl ring was found to be ~53°.

Table IV. Selected Bond Lengths (Å) and Bond Angles (deg) for [**10**](ClO_4) and [**11**](ClO_4)

[**10**](ClO_4)		[**11**](ClO_4)	
Bond Lengths			
Pt–N(1)	2.219(3)	Pt–N(1)	2.15(2)
Pt–N(2)	1.958(2)	Pt–N(2)	1.952(7)
Pt–N(3)	2.030(2)	Pt–N(3)	2.016(6)
Pt–C(13)	2.006(4)	Pt–C(13)	2.02(1)
Bond Angles			
N(1)–Pt–N(2)	79.1(2)	N(1)–Pt–N(2)	79.0(4)
N(1)–Pt–N(3)	105.7(1)	N(1)–Pt–N(3)	106.8(3)
N(1)–Pt–(C13)	159.5(2)	N(1)–Pt–(C13)	161.1(3)
N(2)–Pt–N(3)	175.2(1)	N(2)–Pt–N(3)	174.0(5)
N(2)–Pt–C(13)	80.8(1)	N(2)–Pt–C(13)	82.1(4)
N(3)–Pt–C(13)	94.7(1)	N(3)–Pt–C(13)	92.1(3)

The structures of **10** and **11** were determined by X-ray crystallography. Parts a and b of Figure 3 show the perspective views of **10** and **11**, respectively, featuring some unique examples of donor–acceptor cyclometalated Pt(II) complexes. In both structures, the coordination geometry around Pt(II) is not unusual. One of the phenyl groups of (C⌒N⌒N-dpp) is nearly parallel with the nitrogen base ligand, which is perpendicular to the mean plane defined by the atoms N(1), N(2), C(13), and Pt. The electronic interaction of α-diimines coordinated perpendicularly to the remaining part of the molecule has been discussed.[5a] This electronic insulating property of perpendicularly coordinated pyridine will be encountered in later sections.

The respective Pt–C distances for **10** and **11** [2.006(4) and 2.02(1) Å] are similar to the value of 2.008(24) Å reported for the related [Pt(L)(CH_3CN)](PF_6) (HL = 6-phenyl-2,2′-bipyridine) complexes[17a] as well as to the Pt–C distance of **7**. Replacement of acetonitrile in **7** with para-substituted pyridines unavoidably increases the steric crowding around the metal center. Figure 4 shows the perspective crystal lattice diagrams of **10** and **11**. Although no intermolecular metal–metal stacking interaction is observed in either case, for **11**, there is stacking interaction between the [Pt(C⌒N⌒N-dpp)]$^+$ moiety and an adjacent anthracene unit, the plane to plane separation being 3.58 Å (Figure 4b), which is comparable and shorter than the stacking distance for [Pt(phen)$_2$]Cl_2.[19] For **10**, the shortest separation between the Pt atom and the nearest nitrobenzene moiety in the crystal lattice is over 7 Å.

Properties, Electronic Absorption, and Emission Spectra. As substitution of acetonitrile by 4-methylpyridine has little effect on the emission spectrum of **7**, complex **8** can be considered as the model for understanding the MLCT excited states of these donor–acceptor Pt(II) complexes. Its UV–vis absorption spectrum in acetonitrile shows an intense absorption band at 335 nm ($\epsilon \sim 10^4$) and a shoulder around 380 nm ($\epsilon \sim 10^4$), which are tentatively assigned to the spin-allowed MLCT transitions.[20] There

(19) Hazell, A.; Mukhopadhyay, A. *Acta Crystallogr.* **1980**, *B36*, 1647–1649.

(20) Absorption and luminescence properties of dpp in CH_2Cl_2 have been reported in: Armaroli, N.; De Cola, L.; Balzani, V.; Sauvage, J.-P.; Dietrich-Buchecker, C. O.; Kern, J.-M. *J. Chem. Soc., Faraday Trans.* **1992**, *88*, 553–556. In this reference the emission maxima of free dpp (structured) and protonated dpp (unstructured) are ~370 and ~480 nm, respectively.

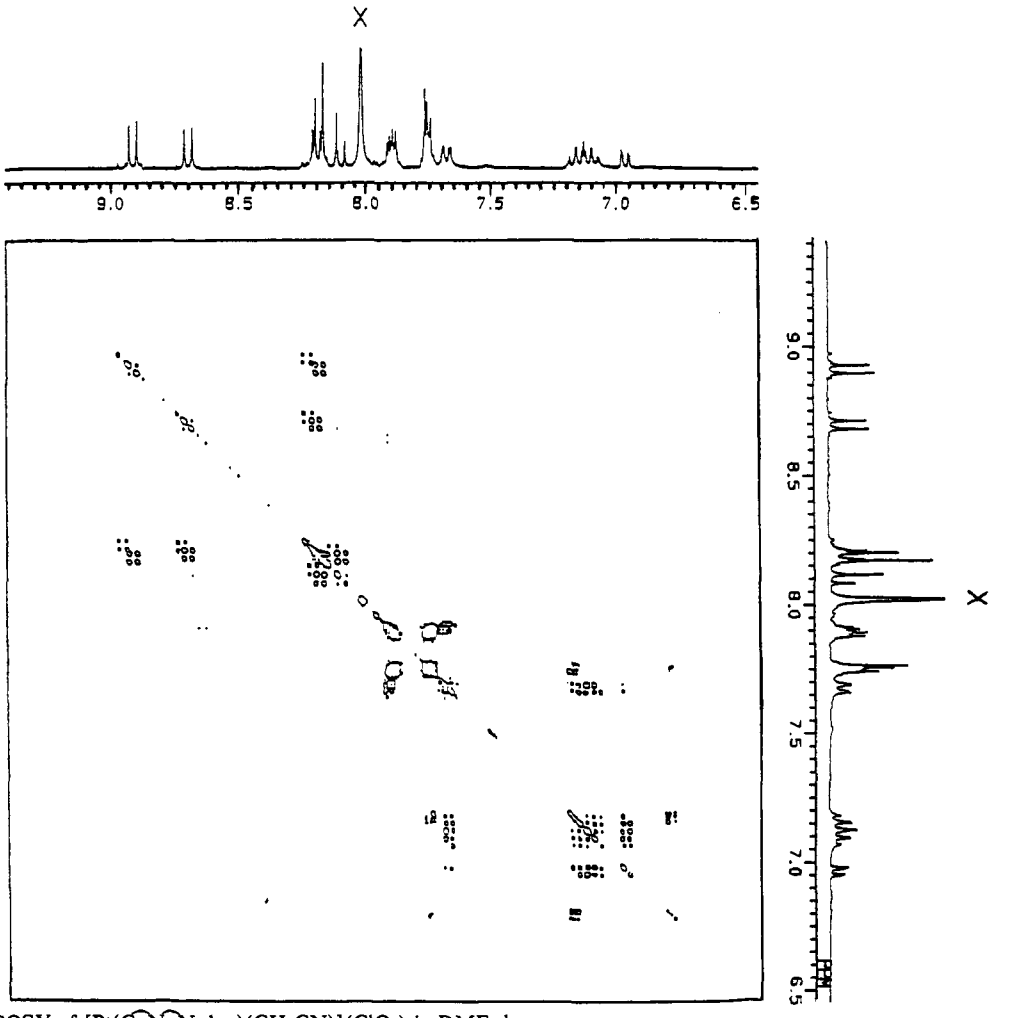

Figure 1. ^1H–^1H COSY of [Pt(C^N^N-dpp)(CH_3CN)](ClO_4) in DMF-d_6.

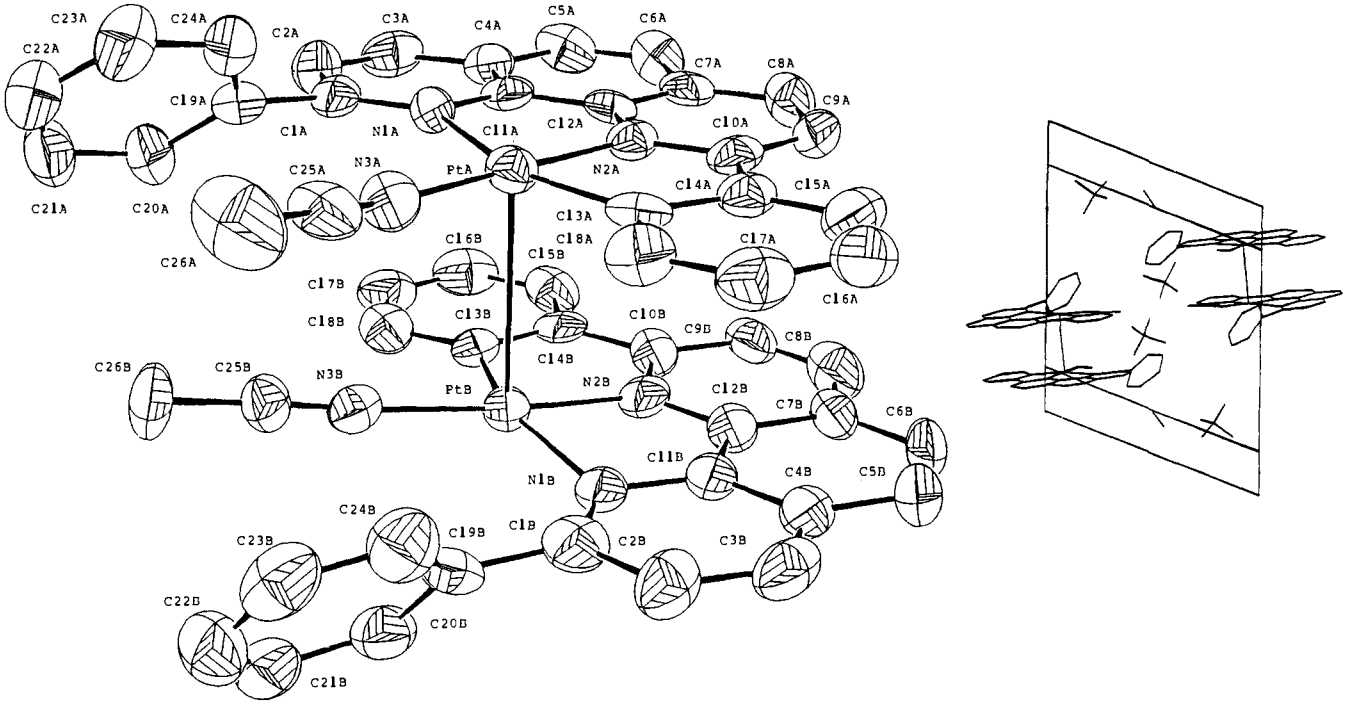

Figure 2. (a, Left) Perspective view and (b, right) crystal lattice diagram of [**7**](ClO_4).

is also some weak absorption tailing from 380 to 450 nm ($\epsilon \leq 10^3$). Previous studies of cyclometalated platinum complexes (Pt(bpy)(bph)[21] and Pt(ppy)$_2$,[5c] where bpy = 2,2′-bipyridine, bph = biphenyl, and ppy = phenylpyridine) have demonstrated solvent dependency of electronic absorptions around 400 nm which has been attributed to charge-transfer transitions.

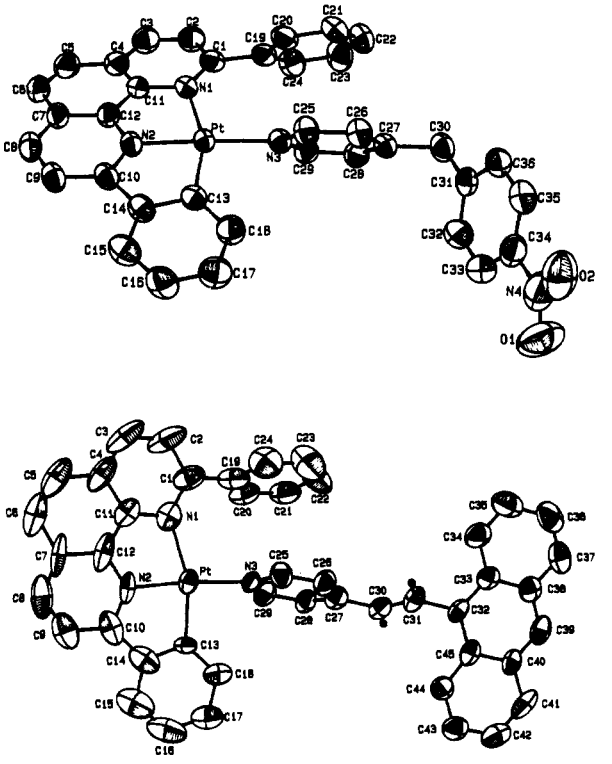

Figure 3. Perspective views of (a, top) [**10**](ClO_4) and (b, bottom) [**11**](ClO_4).

At room-temperature and in degassed acetone, complex **8** shows an intense vibronic structured emission at 530–750 nm upon excitation at 355 nm. The quantum yield is independent of excitation from 350–450 nm. As with other cyclometalated platinum complexes, self-quenching of the excited state has been observed. The Stern–Volmer plot, $1/\tau$ versus concentration of **8**, is linear, giving a lifetime at infinite dilution of 1.55 μs.

With reference to previous work on other cyclometalated Pt(II) complexes,[5a,22] the emission from **8** is suggested to come from an MLCT triplet excited state, ^{3}MLCT. The E_{0-0} energy of **8** is estimated to be 2.4 eV from the onset of emission at 520 nm. The relatively high excited-state energy together with the long lifetime suggests that the excited state of **8** should possess rich photochemistry.

Other complexes such as **9**, **10**, **12**, and **13** show vibronic structured emissions similar to that of **8**, but the lifetimes and quantum yields are modified by the substituents on the pyridine ligands. The photophysical data are summarized in Table V. For complex **12**, fluorescence from the anthracene unit ^{1}An* has also been observed (Figure 5). Several interesting conclusions can be drawn. Complex **9** and **13** have much longer excited state lifetimes and larger emission quantum yields than those of **8** and **12**, respectively. We attribute this effect to the ortho-substituent on the pyridine ligands in **9** and **13**, which would inhibit the approach of the solvent molecule to the platinum atom, thus diminishing the nonradiative decay pathway due to solvent-induced vibrational relaxation. Solvent-induced quenching of the MLCT excited state of transition-metal complexes has previously been noted in the photochemistry of a Cu(I) α-diimine system.[23] Given the coordinative unsaturated nature of Pt(II), it is not unreasonable to speculate that a similar nonradiative decay pathway exists. Thus, a long-lived and emissive excited state of cyclometalated Pt(II) can be achieved with sterically bulky nitrogen-base ligands.

Anthracene is a representative chromophore in organic energy-transfer processes. Descriptions of the photophysical properties of anthracene-containing supramolecules have been reported.[24] It has served as a valuable luminescence probe in fundamental studies of energy transfer in organized media.[25] The choice of anthracene-substituted pyridine as an auxiliary ligand may provide insight into the photophysical properties of cyclometalated platinum(II) complexes.

The emission lifetimes and quantum yields of the MLCT emissions of **8** and **12** are surprisingly similar, indicating no observable intramolecular energy transfer from ^{3}MLCT to ^{3}An* (the rate constant should be less than 10^5 s^{-1}). This is quite different from that of the system $[Ru(bpyCH_2OCH_2An)_3]^{2+}$ ($bpyCH_2OCH_2An$ = 4-((9-anthrylmethoxy)methyl)-4′-methyl-2,2′-bipyridine),[26] where a constant of $>2 \times 10^8$ s^{-1} has been found for the intramolecular energy transfer from the ^{3}MLCT state of Ru(II) to ^{3}An*.

Intramolecular Energy Transfer and Antenna Effect of the Anthryl Substituent in Complex 13. Interestingly, the lifetime of the MLCT emission of **13** is about 4 times shorter than that of **9**. Such a decrease in emission lifetime is likely due to intramolecular energy transfer from ^{3}MLCT to ^{3}An*. However, this argument is difficult to prove because the strong emission from the ^{3}MLCT state makes the observation of anthracene phosphorescence and transient absorption of the triplet excited state of anthracene difficult. Emission from the triplet state of organic molecules is rare under ambient conditions. Calculation of the intramolecular energy-transfer rate constant is not appropriate in this case because of the dramatic difference in size and electronic structure of the ortho-substituents in **9** and **13**, which would also affect the nonradiative decay rate constant.

Another interesting finding is that while the emission quantum yield of **12** is independent of the excitation wavelength, that of **13** when extrapolated to infinite dilution is 0.4 ± 0.07 and 0.048 ± 0.005 for excitation at 355 and 450 nm, respectively. Since the anthracene unit absorbs at 355 nm but not at 450 nm, we attribute the difference in emission quantum yield to an antenna effect—enhanced population of ^{3}MLCT due to intramolecular energy transfer from ^{1}An*. As expected, the emission spectrum of **13** does not show any significant anthracene fluorescence in contrast to that shown in Figure 5. The lowering of emission efficiency from the ^{3}MLCT state compared with the case for **9** may be attributed to energy transfer to ^{3}An*. Comparison of the electronic spectra of **12** and **13** reveals no significantly ground-state interaction between the anthryl moiety and the [Pt-C^N^N-dpp]$^+$ moiety in **13**. Only the dynamic phenomenon of energy transfer concerns us here.

Excimer Formation of $[7]_2$* in Dichloromethane.[27] Excited-state deactivation of cyclometalated platinum(II) through an annihilation process has been reported recently.[28] Emission decay kinetics has been found to be laser power dependent. Excimer emission from [Pt(dtbipy)$(CN)_2$] (dtbipy = 4,4′-di-*tert*-butyl-2,2′-bipyridine) and [Pt(4,7-diphenyl-1,10-phenanthroline)$(CN)_2$] in halocarbon solvent has also been observed.[29] In this study, dual emission was observed when a saturated solution of

(21) Cornioley-Deuschel, C.; von Zelewsky, A. *Inorg. Chem.* **1987**, *26*, 3354–3358.
(22) Maestri, M.; Sandrini, D.; Balzani, V.; Chassot, L.; Jolliet, P.; von Zelewsky, A. *Chem. Phys. Lett.* **1985**, *122*, 375–379.
(23) McMillin, D. R.; Kirchhoff, J. R.; Goodwin, K. V. *Coord. Chem. Rev.* **1985**, *64*, 83–92.
(24) (a) Konopelski, J. P.; Kotzyba-Hibert, F.; Lehn, J.-M.; Desvergne, J.-P.; Fagès, F.; Castellan, A.; Bouas-Laurent, H. *J. Chem. Soc., Chem. Commun.* **1985**, 433–436. (b) Mau, A. W.-H.; Sasse, W. H. F.; Creaser, I. I.; Sargeson, A. M. *New J. Chem.* **1986**, *10*, 589–592.
(25) (a) Kimizuka, N.; Kunitake, T. *J. Am. Chem. Soc.* **1989**, *111*, 3758–3759. (b) Ramamurthy, V., Ed. *Photochemistry in Organized and Constrained Media*; VCH: New York, 1991.
(26) Boyde, S.; Strouse, G. F.; Jones, W. E., Jr.; Meyer, T. J. *J. Am. Chem. Soc.* **1989**, *111*, 7448–7454.
(27) For the inorganic exciplex, see: Stacy, E. M.; McMillin, D. R. *Inorg. Chem.* **1990**, *29*, 393–396.
(28) Maestri, M.; Sandrii, D.; von Zelewsky, A.; Deuschel-Cornioley, C. *Inorg. Chem.* **1991**, *30*, 2476–2478.

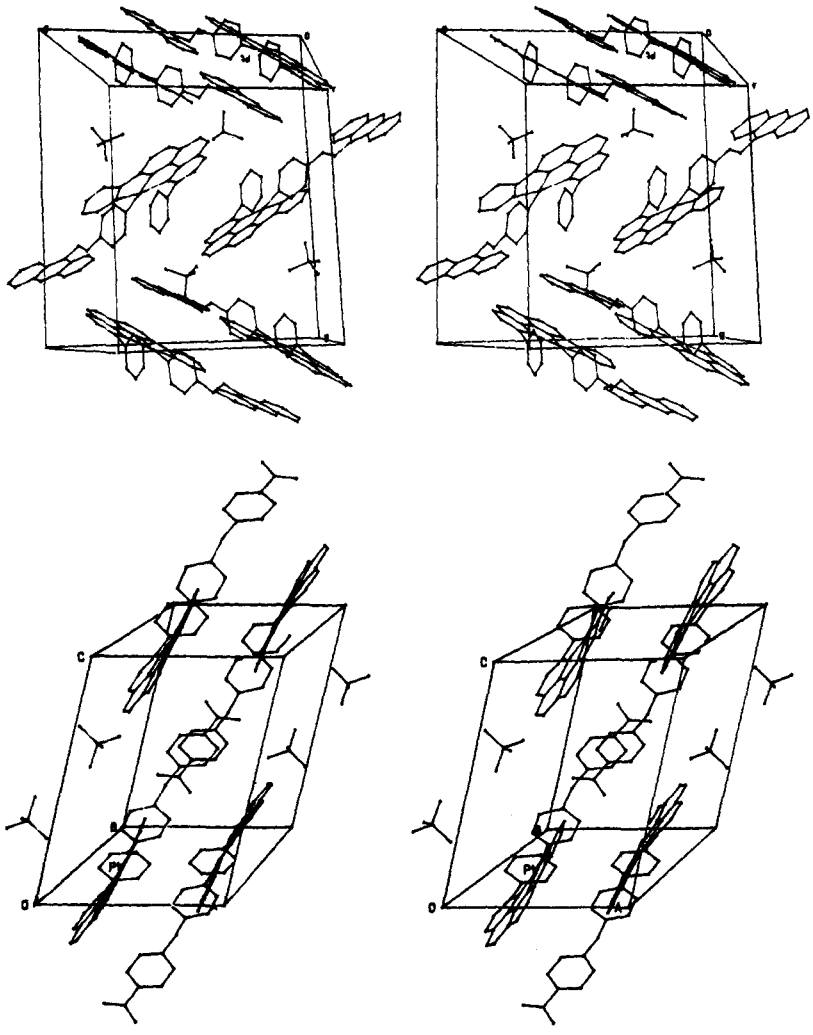

Figure 4. Crystal lattice diagrams of (a, top) [**10**](ClO_4) and (b, bottom) [**11**](ClO_4).

Table V. Lifetimes (τ_0) and Emissino Quantum Yields (ϕ_0)[a] of the Excited MLCT States for **8**, **9**, **12**, and **13** in Acetone[b]

	8	**9**	**12**	**13**
τ_0, μs	1.55	46	1.73	10.4
ϕ_0	0.035	0.30	0.01	0.40 (0.048)[c]

[a] Entries were calculated using the following equations, as the observed lifetimes and emission quantum yields were concentration dependent: $1/\tau = 1/\tau_0 + k_q[Pt]$, $\phi_0/\phi = 1 + \tau_0 k_q[Pt]$. [b] Solutions were degassed with no fewer than three freeze–pump–thaw cycles; excitation was 355 nm. [c] Excitation was 450 nm.

7 in dichloromethane (8.0×10^{-4} mol/dm^3) was excited at 355 nm (see Figure 6A, curve a). The emission can be resolved into monomer emission ranging from 500 to 650 nm (quantum yield = 0.071) and a broad emission centered at ~700 nm (quantum yield = 0.032). Since the electronic spectrum of a concentrated CH_2Cl_2 solution of **7** indicates no ground-state aggregation (see Figure 6B), the ~700-nm emission in Figure 6A should originate from the excimer $[7]_2$* such as that found in other α-diimine–Pt(II) complexes.[30] The origin of this broad emission can also be probed by observing the solid-state emission of **7** which exhibits a similar broad emission around 680 nm (Figure 6A, insert). As has been noted before, **7** retains a dimeric form in the crystalline state with weak Pt–Pt interaction and π–π aromatic interaction between two phenanthroline moieties. However, there is no stacking interaction between individual dimeric units in the crystal lattice. Though one should be cautious when using information from the solid state to discuss substances in different states, the close resemblance of solid emission with the solution emission points to a highly probable structure of $[7]_2$* in CH_2Cl_2.

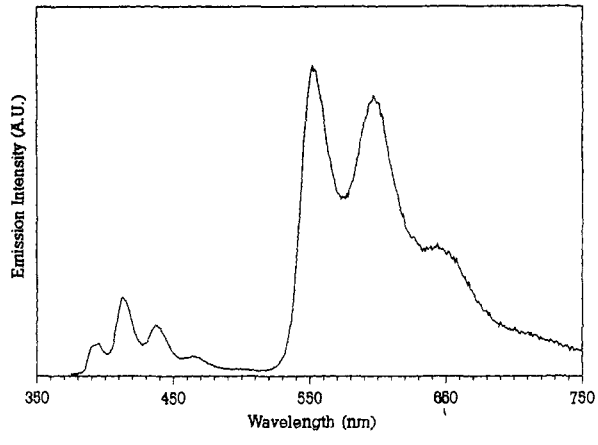

Figure 5. Corrected emission spectrum of **12** (1.7×10^{-5} M in degassed acetone, excitation 355 nm).

The rise time of luminescence in Figure 7 is notably longer than the instrumental *RC* time, indicating consecutive processes[31] as depicted in Scheme I, where [Pt^{II}] stands for **7**. The lifetime

(29) (a) Wan, K.-T.; Che, C. M.; Cho, K. C. *J. Chem. Soc., Dalton Trans.* **1991**, 1077–1080. (b) Kunkely, H.; Vogler, A. *J. Am. Chem. Soc.* **1990**, *112*, 5625–5627.

(30) Miskowski, V. M.; Houlding, V. H. *Inorg. Chem.* **1989**, *28*, 1529–1533.

(31) Demas, J. N. *Excited State Lifetime Measurements*; Academic Press: New York, 1983.

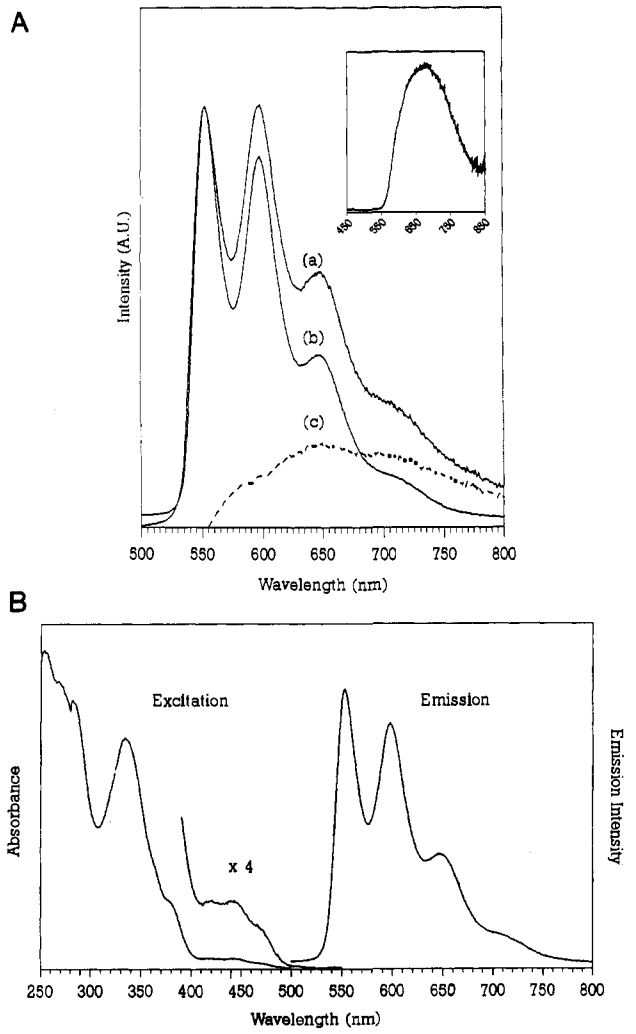

Figure 6. (A, Top) Room-temperature emission spectra of [7](ClO$_4$) in dichloromethane: curve a, dual emission spectrum of 8.0×10^{-4} M 7; curve b, normalized spectrum of 2×10^{-4} M 7; curve c, difference of curve a and curve b; insert, room-temperature emission spectrum of [7](ClO$_4$) in the solid state. (B, Bottom) Emission and excitation spectra of [7](ClO$_4$) in degassed dichloromethane with excitation at 355 nm and emission monitored at 550 nm.

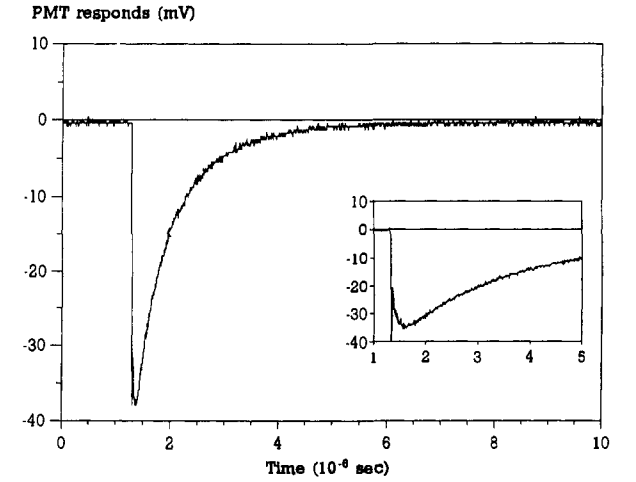

Figure 7. Time-resolved emission spectrum of [7](ClO$_4$) monitored at 706 nm with excitation at 355 nm (8.0×10^{-4} M in dichloromethane).

and quantum yields of 7 are summarized in Table VI. The long lifetime ($\sim 10^{-5}$ s) of excited-state [7]* undoubtedly facilitates excimer formation.

The self-quenching rate constant k_q (6.5×10^8 M^{-1} s^{-1}) can

Scheme I

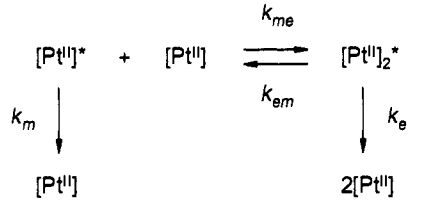

Table VI. Summary of Emission Characteristics of [7](ClO$_4$)[a]

solvent	τ_0, μs	ϕ_0	k_r, s^{-1}	k_{nr}, s^{-1}	k_q, mol^{-1} dm^3 s^{-1}
acetone	8.7	0.16	1.8×10^4	9.7×10^4	1.2×10^9
dichloromethane	14	0.21	1.5×10^4	5.6×10^4	6.5×10^8
dichloromethane	$\tau = 2.6$[b]	$\phi = 0.071$[b]			
(7.5×10^{-4} mol dm^{-3})	$\tau = 0.9$[c]	$\phi = 0.032$[c]	3.6×10^4	1.1×10^6	

[a] Entries of rate constants are calculated from τ_0 and ϕ_0 at infinite dilution except where indicated. τ_0 and ϕ_0 are the lifetime and emission quantum yield at infinite dilution, k_q is the self-quenching rate constant, and k_r and k_{nr} are the radiative and nonradiative decay rate constants, respectively. [b] Monomer emission. [c] Excimer emission.

Scheme II

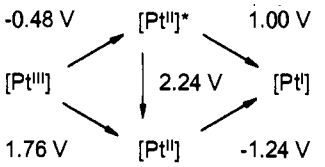

serve as a better estimate of k_{me} if the following deactivation pathways of [Pt^{II}]* are considered

$$[Pt^{II}]^* + [Pt^{II}] \xrightarrow{k_1} [Pt^{II}] + [Pt^{II}]^*$$

$$[Pt^{II}]^* + [Pt^{II}] \xrightarrow{k_2} [Pt^{III}] + [Pt^{I}]$$

$$[Pt^{II}]^* + [Pt^{II}] \xrightarrow{k_{me}} [Pt^{II}]_2^*$$

where k_1 and k_2 represent rate constants for excited-state energy transfer and electron-transfer processes. The magnitudes of k_1 and k_2 would be very small, as both processes are energetically unfavorable. The overlap of absorption and emission spectra of 7 in dichloromethane is small, as evident from Figure 6B. The excited-state electron transfer as described by k_2 is endothermic by 0.8 eV (see the Latimer diagram in Scheme II). Therefore, equilibrium is attained reasonably fast between the excited-state monomer and excimer upon light absorption (6.5×10^8 M^{-1} s^{-1}) when compared with the case for analogous systems (k_{me} in ref 27 was 5.7×10^7 M^{-1} s^{-1}).

Electrochemical Properties of 7 and 8. A reversible reduction process was observed at −1.24 V (vs NHE), and an irreversible oxidation was observed at +1.76 V for complex 7. Interestingly, the substitution of 4-methylpyridine in 8 results in no change in the ease of reduction but increases the oxidation process positively to +1.86 V. This result seems reasonable, as the pyridine ring is orthogonal to the mean plane of [Pt-C^N^N-dpp]$^+$ and thus is not as effective as other auxiliary ligands in back-π-electronic interaction with platinum(II). The increase of oxidation potential may be attributed to an inductive effect.

As a first approximation, the excited-state potential of 7 can be estimated, as depicted in the Latimer diagram (Scheme II). Excited [Pt-C^N^N-dpp]$^+$ is predicted to be a moderately strong photo-oxidant 1.0 V (vs NHE) apart from the kinetic barrier due to structural reorganization. Further characterization of the excited state of [7](ClO$_4$) is in progress.

Conclusion. We have demonstrated that new luminescent donor–acceptor Pt(II) complexes can be easily prepared from **7**. Given the fact that the structure of the auxiliary pyridine ligand can be easily modified, this work defines a new versatile class of organometallic electron donor–spacer–acceptor systems. Attractive features are that a variety of α-diimine-based electron donor/electron acceptors can be used, conformation control can be easily attained, and a closely controlled range of systems can be studied because the electron donor, electron acceptor, spacer, and solvent can all be varied independently. These characteristics provide access to a variety of air-stable, coordinatively unsaturated donor–acceptor metal complexes for studies in molecular recognition and photoinduced electron-transfer and energy-transfer reactions.[32]

(32) Zuleta, J. A.; Burberry, M. S.; Eisenberg, R. *Coord. Chem. Rev.* **1990**, *97*, 47–64.

Acknowledgment. We acknowledge support from The Hong Kong Research Grants Council and The University of Hong Kong. C.-M.C. is thankful for a Visiting Professorship administered by the National Taiwan University.

Supplementary Material Available: Crystal structure data for **7**, **10**, and **11**, including atomic coordinates and isotropic thermal parameters (Tables 1S–3S), complete bond distances (Tables 4S–6S) and angles (Table 7S–9S), anisotropic thermal parameters (Tables 10S–12S), and a summary of crystal data, intensity collection, and structural refinement parameters (Table 16S) (9 pages); observed and calculated structure factors (Tables 13S–15S) (34 pages). Ordering information is given on any current masthead page.